JOURNAL OF GEOPHYSICAL RESEARCH, VOL. 116, C04001, doi:10.1029/2010JC006682, 2011

A wave-based model for the marginal ice zone including a floe breaking parameterization

D. Dumont,[1,2] A. Kohout,[3] and L. Bertino[1]

Received 1 October 2010; revised 10 December 2010; accepted 29 December 2010; published 1 April 2011.

[1] The marginal ice zone (MIZ) is the boundary between the open ocean and ice-covered seas, where sea ice is significantly affected by the onslaught of ocean waves. Waves are responsible for the breakup of ice floes and determine the extent of the MIZ and floe size distribution. When the ice cover is highly fragmented, its behavior is qualitatively different from that of pack ice with large floes. Therefore, it is important to incorporate wave-ice interactions into sea ice–ocean models. In order to achieve this goal, two effects are considered: the role of sea ice as a dampener of wave energy and the wave-induced breakup of ice floes. These two processes act in concert to modify the incident wave spectrum and determine the main properties of the MIZ. A simple but novel parameterization for floe breaking is derived by considering alternatively ice as a flexible and rigid material and by using current estimates of ice critical flexural strain and strength. This parameterization is combined with a wave scattering model in a one-dimensional numerical framework to evaluate the floe size distribution and the extent of the MIZ. The model predicts a sharp transition between fragmented sea ice and the central pack, thus providing a natural definition for the MIZ. Reasonable values are found for the extent of the MIZ given realistic initial and boundary conditions. The numerical setting is commensurate with typical ice-ocean models, with the future implementation into two-dimensional sea ice models in mind.

Citation: Dumont, D., A. Kohout, and L. Bertino (2011), A wave-based model for the marginal ice zone including a floe breaking parameterization, *J. Geophys. Res.*, *116*, C04001, doi:10.1029/2010JC006682.

1. Introduction

[2] The marginal ice zone (MIZ) is the portion of ice-covered seas that is significantly affected by open ocean waves. The MIZ is a complex and highly variable sea ice environment usually appearing as many individual floes of arbitrary shape and made of mixed ice types, from young forming ice to fragmented multiyear ice, depending upon the location and the history of the MIZ. Ocean waves are the primary source of energy for ice breakup in the MIZ and are therefore the main driver determining its properties and extent [*Squire et al.*, 1995]. Swell can penetrate great distances into the ice and potentially transform a large ice sheet into a collection of small individual floes, depending on ice conditions and incident wave energy [*Squire*, 2007]. One major consequence is to reduce the ice resistance to wind and ocean current large-scale stresses. Unlike in the central ice pack, sea ice in the MIZ is much more mobile and fluid. Thus, the presence of ice vortices at the ocean's surface (Figure 1) is a clear indication of the low cohesion and low shear viscosity at the large scale.

[1]Nansen Environmental and Remote Sensing Center, Bergen, Norway.
[2]Now at Institut des Sciences de la Mer, Université de Québec à Rimouski, Rimouski, Quebec, Canada.
[3]National Institute of Water and Atmospheric Research, Christchurch, New Zealand.

0148-0227/11/2010JC006682

[3] Many authors attempted to describe ice dynamics in the MIZ using either simple [*Røed and O'Brien*, 1981, 1983; *Hakkinen*, 1986] and sophisticated ice rheologies [*Shen et al.*, 1986, 1987; *Feltham*, 2005]. They all recognized the role of waves play in ice dynamics but did not explicitly take them into account. The work of *Shen et al.* [1987] is a good example of a rheology formulation that implicitly considers the role of waves. They first consider sea ice as a collection of circular floating disks of constant diameter that collide with each other thanks to the wave-induced random motion. The fluctuation velocity is set constant, uniform, and significantly larger than the large-scale deformation, assumptions made in order to obtain an analytical expression for the stress tensor. The resulting non-Newtonian fluid has lower strength, cohesion and viscosities compared to the viscous-plastic (VP) formulation [*Hibler*, 1979], in agreement with the dynamical properties of the MIZ. Waves are implicitly included in the fact that sea ice is fragmented and that floes are animated by random motion. Ideally, if a collisional rheology is to be implemented in a sea ice model, waves would have to be considered explicitly, although an empirical method would also be possible.

[4] Waves also impact sea ice thermodynamics. By breaking up the floes, they can accelerate ice melting during summer due to enhanced lateral melting for small floes [*Steele et al.*, 1989; *Steele*, 1992], and promote ice formation during winter by creating interstices between ice floes where new ice can form. Waves can affect ice growth and heat fluxes in polynya and near the ice edge [*Lange et al.*, 1989],

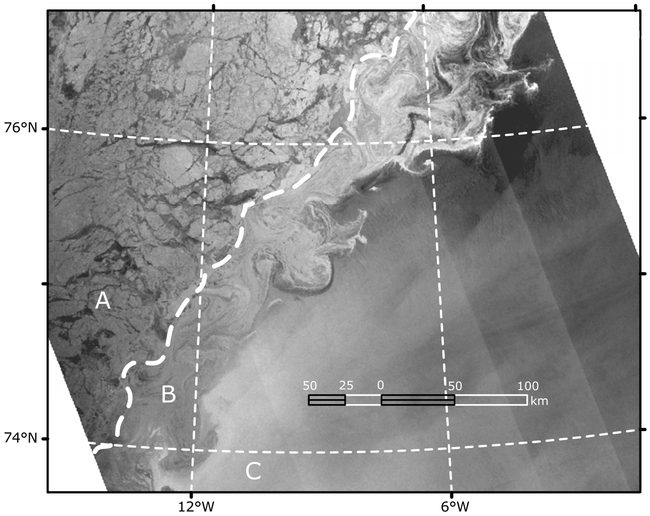

Figure 1. Synthetic aperture radar (SAR) image of Fram Strait on 16 January 2010. The thick dashed line marks the transition between the marginal ice zone (MIZ, area B, where floes are undistinguishable) and the central ice pack (area A, where floes are large enough to be distinguished). Area C represents open water. The width of area B varies from 25 to 100 km.

and significantly alter ocean mixing and air-sea momentum transfer [*Janssen*, 2004; *Jenkins*, 2007].

[5] In the Antarctic, the MIZ surrounds the Southern Ocean ice cover, which is continuously impacted by ocean swell from the Indian, Atlantic and Pacific Oceans. In the Arctic, the MIZ is mainly encountered in the marginal seas, such as the Nordic Seas, the Barents Sea, the Beaufort Sea and the Labrador Sea. By strongly scattering the wave energy, thick multiyear ice prevents swell from penetrating deeply into the Arctic ice pack. However, with the recent changes affecting Arctic sea ice, the Arctic has more ice-free seas exposed to wind. Consequently, waves gain more energy from the extended fetch and can therefore penetrate further into the ice pack. With the increasing human presence in the Arctic, waves pose security and safety issues. As marginal seas are targeted for oil and gas exploitation, understanding and predicting ocean waves and their effects on sea ice become crucial for structure design and for real-time safety of operations. The juxtaposition of waves and sea ice represents a risk for personnel and equipment deployed on ice, and may complicate critical operations like a platform evacuation. The risk is difficult to evaluate because there are no long-term observations of waves in ice, swell events are difficult to predict from local conditions, ice breakup can occur on very short timescales [*Liu and Mollo-Christensen*, 1988; *Marko*, 2003], and wave-ice interactions are beyond the scope of current forecasting models. For these reasons, the need to incorporate wave-ice interactions in sea ice–ocean forecasting models is becoming a pressing issue.

[6] The main objective of this paper is to design and test a method to calculate the floe size distribution as waves propagate through and break up sea ice into small floes. This method aims at introducing floe size as a prognostic variable in sea ice models for the inclusion of MIZ processes. In this paper, two processes are identified, parameterized, and tested in both idealized and realistic conditions: (1) the attenuation of gravity waves in sea ice and (2) floe breaking due to the action of waves.

[7] In the former case, we take advantage of the significant advances made in the mathematical modeling of waves in ice-covered seas. The theory that considers ice floes as floating elastic plates, formulated by *Wadhams* [1986], was solved by *Meylan and Squire* [1994] in two dimensions. The three-dimensional solution of this problem began with the work of *Masson and Leblond* [1989] and was subsequently developed by others [*Meylan and Squire*, 1996; *Meylan et al.*, 1997; *Meylan*, 2002; *Bennetts et al.*, 2010]. In *Squire*'s [2007] review, it is argued that the level of realism of today's models encourages to use and test them in more realistic problems. Here we use the model of *Kohout and Meylan* [2008] developed for the MIZ.

[8] To account for floe breaking, we use an approach that differs from the elastic plate theory, but still recognize the mechanical properties of sea ice. This approach takes into account experimental knowledge about the flexural strength of sea ice, which is not explicitly included in the elastic plate theory. Finally, these two processes are combined and implemented in a numerical framework commensurate with typical ice-ocean models, in order to facilitate further implementation in climate or operational coupled models. A functional definition of the MIZ follows naturally and is used to estimate its extent.

[9] The outline of the paper is as follow. The model and its components are described in section 2. In section 3, the sensitivity of the model to parameters and environmental conditions is assessed. Then, the model is applied on the output of a high-resolution ice-ocean model of Fram Strait. Based on these results, an empirical method is proposed to segregate dynamical regimes in sea ice models without having to include waves explicitly. A conclusion is provided in section 4.

2. Model

2.1. Incident Wave Spectrum

[10] Ocean waves are forced by the wind and their energy is a function of wind speed and fetch, i.e., the distance over which the wind blows. Short waves are first produced and grow into longer waves due to dispersion and wave-wave interactions. Under sustained wind conditions, waves grow until generation is balanced by dissipation (e.g., through wave breaking). A fully developed sea is then achieved. Transient sea states are referred to as partially developed seas or growing seas. When wind weakens or waves travel away from their site of generation, the sea is said to be decaying. Energy density spectra are used to characterize the sea state, which can be retrieved from times series of sea surface elevation or produced by a spectral wave model. Typically, the wave spectrum can be characterized by a finite set of parameters such as the peak period T_p and the significant wave height H_s, defined as the average height (from trough to crest) of the 1/3 highest waves in a given record [*World Meteorological Organization* (*WMO*), 1998]. Semiempirical functions based on these two parameters have been proposed to characterize the wave spectrum of different sea

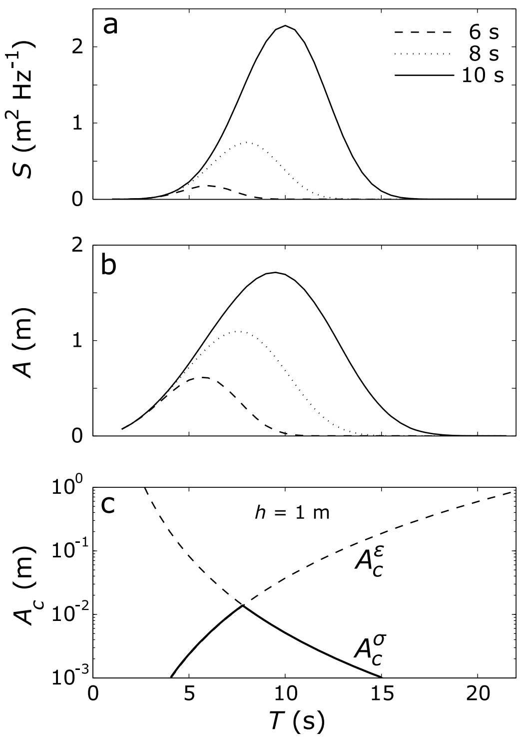

Figure 2. (a) The Pierson-Moskowitz wave energy spectrum and (b) the corresponding wave amplitude spectrum for different peak periods, T_p = 6, 8, and 10 s. (c) Strain and stress yield amplitude (A_c^ε and A_c^σ, respectively) above which waves are breaking a 1 m thick ice plate. The solid line represents the combination of the two modes of failure, i.e., the minimum yield amplitude.

states. The Pierson-Moskowitz spectrum S_P [*Pierson and Moskowitz*, 1964] describes a fully developed seas using the peak period as the only free parameter. It was obtained from wave measurements in the North Atlantic and is given by

$$S_P(T) = 8.1 \times 10^{-3} g^2 \left(\frac{T}{2\pi}\right)^5 e^{-1.25\left(T/T_p\right)^4}, \tag{1}$$

where T is the period and g = 9.81 m^2 s^{-1} is the gravitational acceleration. To represent a broader range of partially developed seas, the two-parameter Bretschneider spectrum S_B [*Ochi*, 1998] is used and includes a dependence on both H_s and T_p. It is defined by

$$S_B(T) = \frac{1.25 H_s^2 T^5}{8\pi T_p^4} e^{-1.25\left(T/T_p\right)^4}. \tag{2}$$

S_P is obtained from (2) by letting $T_p = 5\pi\sqrt{H_s/g}$. A real sea is the result of an infinite number of superimposing waves with different periods, speeds, amplitudes and directions. A wave spectrum gives averaged information about the spectral distribution of the wave energy, which is proportional to the square of the amplitude. Although it can be written using continuous functions like those mentioned above, the wavefield is defined in a discretized spectral domain, whether it is provided by a wave model or calculated from wave data using Fourier transforms. By integrating S over a range of periods, one obtains information about the average amplitude of this group of waves. In a discretized spectral domain,

$$A_w = \sqrt{2 S_w \omega_w} = \sqrt{4\pi S_w / T_w} \tag{3}$$

can be regarded as the mean amplitude for a given interval, say between $T_w - \Delta T$ and $T_w + \Delta T$ [*WMO*, 1998]. By choosing ΔT small enough, one can resolve the spectrum and obtain a good estimation of the mean amplitude. Figure 2 shows the wave amplitude spectrum corresponding to the Pierson-Moskowitz spectrum with different T_p values. The real amplitude, however, results from the superimposition of many waves with different phases and directions in space and time. Because selective attenuation tends to narrow the spectrum toward low frequencies and dispersion tends to decorrelate individual waves that travel with different speeds, this effect is more significant near the ice edge and becomes less important as waves propagate in sea ice. Although possibly significant, it is neglected here since the goal is to assess the validity and sensitivity of a simple approach.

2.2. Wave Propagation and Attenuation

[11] Theoretical and observational studies show that wave energy is strongly attenuated in sea ice, with an increasing exponential decay with increasing frequency. Wave measurements from *Wadhams et al.* [1988] provide evidence that wave scattering occurring at floe edges is the dominant mechanism for energy loss in the MIZ. This is further supported by a reasonably good correspondence between wave measurements and the results from a scattering model of *Kohout and Meylan* [2008] (hereby referred to as KM).

[12] The amplitude of gravity waves traveling in sea ice is small relative to the wavelength, such that linearity can reasonably be assumed and each wave of period T_w (w = 1,2,3..) can be considered separately and independently. In a one-dimensional configuration, a constant direction of propagation is assumed, from the ice edge inward. The wave amplitude is advected explicitly using an upwind scheme of the form

$$A_{w,j}^{n+1} = A_{w,j}^n + \frac{a_w \Delta t}{\Delta x}\left(A_{w,j-1}^n - A_{w,j}^n\right), \tag{4}$$

where a_w is the group speed, A_w the amplitude of the wave w, and j and n are used for space and time indexing, respectively. Δx is the grid cell size and Δt is the time step. Wave attenuation is represented by

$$A_{w,j}^{n+1} = A_{w,j}^{n+1} \exp\left[-\alpha_{w,j} a_w \Delta t\right] \tag{5}$$

and is applied after the advection at each time step. α is an attenuation coefficient in m^{-1} that depends on the wave period and the ice thickness. To compute α, the two-dimensional (one horizontal and one vertical) wave scattering model of KM, specifically developed for the MIZ, is used. In this model, floes are treated as floating elastic plates with prescribed length and thickness. Any other viscous effects potentially attenuating waves are neglected. The model solves for the sum of reflected and transmitted waves at each floe interface and the attenuation is obtained by taking the ratio

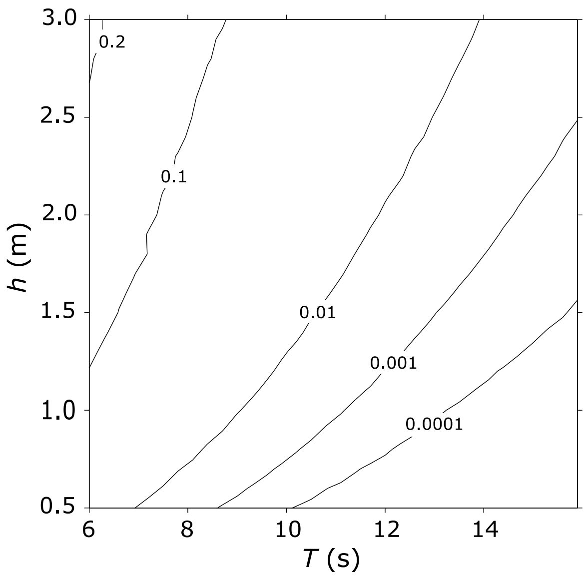

Figure 3. Dimensionless energy attenuation coefficient $\tilde{\alpha}$ (per floe) given by the model of *Kohout and Meylan* [2008] as a function of ice floe thickness and wave period. The domain of validity is restricted to wave periods between 6 and 16 s.

between transmitted and incident wave energy. To average out resonance effects, a Monte Carlo method is used to compute the energy attenuation coefficient for a large number of floes with their lengths obeying a Rayleigh distribution. KM's results support the idea that the wave energy decays exponentially with the the number of floes N, i.e., $E \sim E_0 e^{-\tilde{\alpha}N}$, with an attenuation coefficient that is independent of the floe length for floes larger than ~20 m, for wave periods between 6 and 16 s [*Kohout*, 2008]. When floes are smaller than 20 m, i.e., a fraction of the wavelength, they do not bend significantly and the reflection is reduced. If attenuation should occur for small floes, other mechanisms that are not included in KM's model must be included. The dimensionless energy attenuation coefficient $\tilde{\alpha}$ is converted to a dimensional amplitude attenuation coefficient using $\alpha = c\tilde{\alpha}/2\overline{D}$, where c is the ice concentration and $\overline{D}$ is the mean size of the floes over the traveled distance $a_w \Delta t$. An expression for the mean floe size is derived later in this paper from a floe size distribution. The factor 2 in the denominator comes from the fact that the wave energy is proportional to the square of the amplitude. Figure 3 shows how $\tilde{\alpha}$ varies with wave period and ice thickness according to KM.

[13] A flexural gravity wave has a different dispersion relation than the corresponding ice-free gravity wave, i.e., a different speed and wave number. In a MIZ, waves alternatively travel through ice-free water and through ice floes. In this study, we use the ice-free deep water dispersion relation given by $\lambda = gT^2/2\pi$ [*WMO*, 1998]. The change in the wavelength between an ice-free and an ice-coupled flexural gravity wave is significant only for waves shorter than 10 s for 1 m thick ice [*Wadhams*, 1986]. To give an idea of the discrepancy, for $T = 6$ s, the wavelength increases from ~60 m to ~90 m for an ice-coupled wave.

[14] Moreover, from (4) and (5), one can see that the wave speed only affects the time required for the wave to travel a certain distance. If boundary conditions are kept constant, the final waves-in-ice spectrum at one particular point is independent of the speed. However, during model integration, we make sure that waves are all advanced simultaneously so that the cumulative effect on the ice cover will be taken into account by the whole spectrum. In other words, the spectral loop is inside the spatial loop, which is inside the time loop.

2.3. Floe Breaking Parameterization

[15] Sea ice growth follows several development stages, from grease ice, to pancake ice and finally to a consolidated ice cover. *Shen et al.* [2001] provide a good description of these stages and highlight the role waves are playing at each stage. They describe a conceptual model for pancake ice formation and derive an expression for the limiting diameter in the presence of a wavefield, which is verified experimentally by *Shen et al.* [2004]. The limiting size of pancakes is mainly controlled by tensile stresses induced by the horizontal differential drag imposed by waves. The maximum diameter is typically 1 m and only short waves (1–2 s) have a significant impact on this type of ice. As sea ice grows thicker and harder, wave-induced tensile stresses are exceeded by flexural stresses.

[16] The flexural response of ice floes of finite sizes has been described following different approaches [*Timoshenko et al.*, 1974; *Goodman et al.*, 1980], including numerical modeling [*Squire*, 1981], but no complete analytical description exists so far. Floe breaking due to waves is further complicated by the very high variability of ice mechanical properties influenced by the microstructure (e.g., grain size, crack density, liquid water content) and the strain history [*Wadhams*, 1986]. To derive a floe breaking parameterization, we combine two ways of measuring bending failure, each characterized by a a critical value: a critical strain and a critical stress (strength). These two approaches are not based on the elastic plate theory and thus cannot be considered as a complete and coherent description of the flexural response of an ice floe. Instead, ice is first considered as a flexible material (no rigidity) that fails when the flexural strain limit is reached and a first criterion is derived. Secondly, ice is considered as a very rigid material where cavitation and submergence are both allowed. In that configuration, flexural stresses appear due to gravity and buoyancy forces and ice fails when the flexural strength is reached. These two criteria are computed separately and then merged to form a low-pass filter function for the floe size distribution.

2.3.1. Strain Failure

[17] The flexural strain is defined as

$$\varepsilon = \frac{h}{2} \frac{\partial^2 \eta}{\partial x^2}, \tag{6}$$

where η is the sea surface elevation, h is the ice thickness and x is the horizontal distance. We suppose that the ice plate is finite, that the wavelength and amplitude of the wave are the same as in open water, and that the plate conforms to the wave profile (Figure 4, middle). For a sinusoidal wave profile $\eta = A\sin(kx - \omega t)$, the maximum strain is $\varepsilon = hAk^2/2$ and the distance between two consecutive maxima is $\lambda/2$. The yield amplitude, i.e., the amplitude that will make the ice fail, is

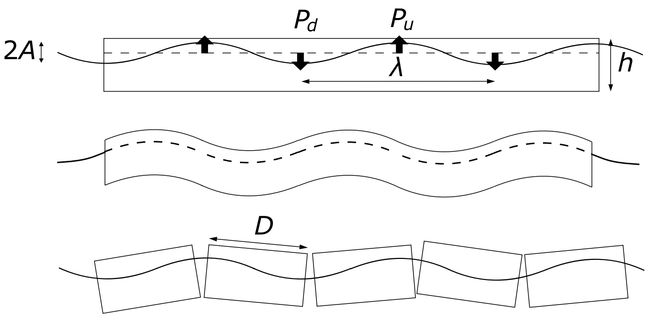

Figure 4. Schematic representation of the two bending failure mechanisms considered for an ice plate of thickness h and for a wave of amplitude A. (top) If the ice plate is considered rigid, upward and downward forces are sequentially applied separated by a distance $\lambda/2$ and a stress yield criterion applies. (middle) If the plate bends following the wave profile, a strain criterion is used to determine floe breaking. (bottom) When ice breaks, it produces floes having a maximum size $D = \lambda/2$.

obtained when the strain reaches the strain yield limit ε_c and is given by

$$A_c^\varepsilon = \frac{\varepsilon_c \lambda^2}{2\pi^2 h}. \tag{7}$$

The strain is linearly proportional to the thickness and inversely proportional to the square of the wavelength. For short waves, smaller amplitudes are thus required to break the ice (Figure 2). This mechanism is only effective near the ice edge because of the rapid decay of short waves.

2.3.2. Stress Failure

[18] When a flexural stress is applied on sea ice, a certain amount is released through strain and the remaining goes into the energy at the scale of ice crystals for maintaining the integrity of the ice body. By using the proper instrumentation and experimental design, it is possible to measure both the strain and the stress at failure. By considering sea ice as flexible enough to conform to the wave profile, we have been able to determine a yield criterion based on the knowledge of the strain at failure. Now, we consider sea ice as a rigid material, calculate the stress imposed by a passing wave, and take advantage of the fact that we know the stress at failure (or flexural strength), to derive a second complementary criterion. For this, we consider an ice plate of constant thickness floating on a sinusoidal sea surface height $\eta = A\sin(kx)$ (Figure 4, top). It is assumed that the ice plate is many times longer than the wavelength so that it rests horizontally in isostatic equilibrium and parallel to the mean sea surface level. At a wave crest, a portion of the sea ice plate is submerged beyond equilibrium and a net upward force P_u due to buoyancy is applied. At a wave trough, the emerged portion increases the apparent weight and a net downward force P_d is applied. The upward force is the excess of buoyancy proportional to ρ_{w}, the downward force is the excess of weight proportional to ρ_{ice}, and $P_u = P_d$ in order to preserve equilibrium. P_u (P_d) is obtained by integrating over the portion of the wave profile where the upward (downward) force is acting. Because $\rho_{\mathrm{w}} \neq \rho_{\mathrm{ice}}$, the integration must be done over a distance smaller than $\lambda/2$ for P_u and larger for P_d, which unnecessarily complicates the solution. Instead, we average by integrating over a half cycle while considering that $P = (|P_u| + |P_d|)/2$ is acting both at crests and troughs. In this way,

$$P = \frac{gA}{2}\left(\rho_{\mathrm{w}}\left|\int_0^{\lambda/2}\sin(kx)dx\right| + \rho_{\mathrm{ice}}\left|\int_{\lambda/2}^{\lambda}\sin(kx)dx\right|\right) = \frac{g\overline{\rho}A\lambda}{\pi}, \tag{8}$$

where $\overline{\rho} \equiv (\rho_{\mathrm{w}} + \rho_{\mathrm{ice}})/2$, $\rho_{\mathrm{w}} = 1025$ kg m^{-3} is the seawater density, $\rho_{\mathrm{ice}} = 922.5$ kg m^{-3} is the sea ice density, and P is a force per unit distance.

[19] To obtain the flexural stress produced by alternating vertical forces, we use the similarity between this configuration and the so-called three-point flexural test setup. This setup involves placing a rectangular beam of thickness h and width b on two supports separated by a distance L. A force F is applied in the center between the supports. The flexural stress σ is then obtained with the following equation [*Schwarz et al.*, 1981]

$$\sigma = \frac{3FL}{2bh^2}. \tag{9}$$

The flexural strength of the material is the flexural stress at which the beam fails or fractures. Substituting (8) in (9) knowing that P is equivalent to F/b, and replacing L by $\lambda/2$, the flexural stress for a wave traveling through an ice plate is written as

$$\sigma = \frac{3g\overline{\rho}A\lambda^2}{2\pi h^2}. \tag{10}$$

Inverting (10) and replacing σ by the flexural strength σ_c leads to

$$A_c^\sigma = \frac{2\pi h^2 \sigma_c}{3g\overline{\rho}\lambda^2}. \tag{11}$$

[20] The effective yield amplitude for arbitrary ice and wave conditions would be given by $A_c = \min(A_c^\varepsilon, A_c^\sigma)$. Again, the two yield criteria are based on two ways of considering the same failure mechanisms, bending failure, that consider two extreme behaviors of sea ice which are both physical. Despite its simplicity, the derivation of the stress failure criterion is done here for the first time and differs from the elastic plate theory with which it should eventually be compared. A noticeable difference is the fact that the stress failure criterion allows cavitation and submergence which is not assumed in the elastic plate theory.

[21] By using the deep water dispersion relation (where $\lambda \propto T^2$), one sees that $A_c^\sigma \propto h^2/T^4$ and $A_c^\varepsilon \propto T^4/h$. This is shown in Figure 2c where the yield amplitude is plotted as a function of the wave period. Strain failure dominates for short waves, where the sea level curvature is maximal. Stress failure dominates for long waves and when stresses between two consecutive wave crests are likely to break even for small amplitude, which is intuitively sensible. If very long swells ($T >$ ~20 s) effectively break the ice, the distance between cracks is also very long and may not necessarily transform the ice cover into a marginal ice zone. Short waves will produce small floes, but, as they are more strongly attenuated than long waves, they will not significantly affect the extent of the marginal ice zone. Thus, the most influential waves for the

marginal ice zone are the ones in the medium range (approximately 6 to 16 s), in line with observations [*Haskell et al.*, 1996].

2.3.3. The Effect of Fatigue

[22] When ice is repeatedly put under stress like in the presence of a wave train, failure can occur when the stress is below the limit value. This property is known as the material fatigue. If there exists a stress below which the material maintains its integrity and resists failure, this limit is called the endurance limit. In sea ice, the endurance limit has been estimated to be approximately 60% of the flexural strength [*Langhorne et al.*, 1998]. Consequently, we choose here to simply parameterize the effect of fatigue by replacing σ_c and ε_c by their endurance limit $\mu\sigma_c$ and $\mu\varepsilon_c$, respectively, with $\mu \simeq 0.6$. *Langhorne et al.* [1998] found that $\mu\varepsilon_c \simeq 3 \times 10^{-5}$. To estimate σ_c, *Timco and O'Brien* [1994] have compiled more than two thousand measurements. Values range from 0.25 to 1.0 MPa depending on the brine content, the ice temperature, the measurement method, and the size of the beam of ice used. A value of 0.67 MPa is used throughout the remainder of this paper unless otherwise specified.

[23] Using the elastic plate theory of *Goodman et al.* [1980], *Wadhams* [1986] estimates that a 12 s wave has a critical amplitude A_c = 7 cm in 3 m thick ice and produces floes with a maximum size of 200 m, with the floe size decreasing with increasing wave amplitude. Our parameterization gives results in the same order of magnitude with A_c = 3 cm and an amplitude-independent maximum floe size of 112 m. The former uses the elastic plate theory and consider ice-coupled flexural gravity waves, but neglects buoyancy effects considered in the present work. Moreover, the latter is expressed in much simpler terms and therefore easier to implement in a numerical model.

2.4. On the Floe Size Distribution

[24] To calculate the dimensional attenuation coefficient α, an estimation of the mean floe size is required. This is possible only if the floe size distribution is known. The floe breaking parameterization derived in section 2.3.3 can be viewed as a truncation scheme that sets an upper limit $D_{\max}$ to a floe size distribution. A lower limit is set to a value $D_{\min}$ = 20 m approximately corresponding to the onset of wave scattering in KM's model. This value is independent of floe thickness and wave period. The question we ask now is how are floe sizes distributed between these limits? When fragmentation, or crushing, is the dominant process affecting the fragment size distribution of a material, the size distribution can be constructed using a renormalization group method [*Turcotte*, 1986; *Palmer and Sanderson*, 1991]. For sea ice the floe size distribution in a MIZ generally follows a power law of the form $N(D) \approx D^{-\gamma}$ with $0 < \gamma < 2$ [*Rothrock and Thorndike*, 1984; *Toyota et al.*, 2006, 2011]. This method is used here to find an expression for the mean floe size when the extrema of the distribution are known. A detailed description of the method is given by *Toyota et al.* [2011] and references therein, but a part of the analysis is repeated here to demonstrate the inclusion of the limit values ($D_{\min}$, $D_{\max}$).

[25] Let us consider a square area of dimension Δx separated in N_0 squares of dimension $D_{\max}$. The squares represent ice floes broken by waves. We suppose that other random processes such as floe-floe collisions and higher-order sea surface slopes created by the combination of multiple waves will further fragment the floes. Following the renormalization group method, floes of size $D_{\max}$ are then fragmented into ξ^2 floes of equal size $D_{\max}/\xi$ with a probability $f\,(0 \leq f \leq 1)$. ξ is an integer larger or equal to 2 which determines the number of pieces each floe will be fragmented into. After the first fragmentation step, the number of floes of size $D_{\max}$ is $\tilde{N}_0 = (1-f)N_0$ and the number of floes of size $D_{\max}/\xi$ is $N_1 = \xi^2 f N_0$. If this step is repeated m times, the number of floes of size $D_{\max}/\xi^m$ is $\tilde{N}_m = (1-f)(\xi^2 f)^m N_0$. By imposing a lower limit to the floe size, the number of fragmentation steps M is limited to

$$M = \left[\log_\xi (D_{\max}/D_{\min})\right]. \tag{12}$$

The minimum floe size does not mean that there are no smaller floes, but that floes smaller than $D_{\min}$ do not contribute significantly to scattering. The mean floe size is calculated from the distribution $\tilde{N}_m(D_m)$ as

$$\overline{D} = \frac{\sum_{m=0}^{M} (\xi^2 F)^m \xi^{-m} D_{\max}}{\sum_{m=0}^{M} (\xi^2 F)^m}. \tag{13}$$

If $D_{\max}$ = 200 m, $D_{\min}$ = 20 m, f = 0.9, and ξ = 2, we obtain M = 3 and a mean floe size $\overline{D}$ = 36 m.

[26] The probability f that a floe will break is interpreted as the fragility of the floes [*Allegre et al.*, 1982; *Turcotte*, 1986]. The more fragile they are the more likely they will break in smaller pieces. The concept of fragility can vary according to a number of factors. Values of f have been calculated in many different regions at different times during the year. They are consistently higher during the melt season [*Steer et al.*, 2008] and decrease with distance [*Toyota et al.*, 2011]. Here, a constant value f = 0.9 is adopted for simplicity.

2.5. Model Step Sequence

[27] Here we summarize how the model operates and how the different components described previously are organized in the integration sequence. Table 1 provides a list of all model parameters and variables with their units and values.

[28] 1. The numerical grid is set up with one spatial dimension and one spectral dimension. The spectral domain covers periods from 6 to 15.9 s separated by 0.3 s intervals. The spectral discretization will dictate how floe size is discretized since it is calculated as half the wavelength of the smallest destructive wave. Sea ice concentration and thickness are interpolated on the grid.

[29] 2. Being only period dependent, wave speed and wavelength are initialized before the integration. The amplitude is set to zero initially for all waves, while floe size is set to 500 m. This value is chosen in order to simulate a background attenuation due to leads, cracks, ridges and other inhomogeneities in rigid plastic ice conditions. Wave forcing is specified as a boundary condition such that $A^n_{w,j=1} = \sqrt{2S_w\omega_w}$. Finally, the yield amplitude A_c is calculated as a function of ice thickness and wave period.

[30] 3. The integration is further divided in five substeps. First, wave amplitude is advected. In order to perform the attenuation step, the dimensionless attenuation coefficient is retrieved from a lookup table and converted into a dimensional coefficient using the information about the maximal floe size. The yield criterion is tested to decide whether the ice is broken. If the ice is unbroken, $\overline{D} = D_{\max}$. If the wave

Table 1. Model Parameters and Variables

Parameter	Symbol	Value
Grid cell size	Δx	5 km
Time step	Δt	400 s
Wave period increment	ΔT	0.3 s
Flexural strength	σ_c	0.67–0.95 MPa
Flexural strain endurance limit	$\mu\varepsilon_c$	3×10^{-5}
Minimum floe size	$D_{\min}$	20 m
Fragmentation factor	ξ	2
Fatigue	μ	0.6
Ice fragility	f	0.9
Ice density	ρ_{ice}	922.5 kg m^{-3}
Seawater density	ρ_w	1025 kg m^{-3}
Gravitational acceleration	g	9.81 m s^{-2}
Variable	**Symbol**	**Units**
Wave phase speed	a	m s^{-1}
Wave group speed	a_g	m s^{-1}
Wavelength	λ	m
Significant wave height	H_s	m
Peak period	T_p	s
Adimensional attenuation coefficient	$\tilde{\alpha}$	dimensionless
Dimensional attenuation coefficient	α	m^{-1}
Ice thickness	h	m
Ice concentration	c	dimensionless
Sea surface height	η	m
Wave amplitude	A	m
Stress yield amplitude	A_c^{σ}	m
Strain yield amplitude	A_c^{ε}	m
Effective yield amplitude	A_c	m
Maximum floe size	$D_{\max}$	m
Average floe size	$\overline{D}$	m

has fragmented the ice cover in a previous time step, then $\overline{D}$ is obtained using equation (13). Attenuation is performed and the updated amplitude is compared with the yield amplitude to determine if the new wave will break up the ice and hence if the floe size must be updated, i.e., further reduced. If not, $D_{\max}$ remains unchanged.

[31] 4. The integration is stopped after the slowest wave has crossed the entire domain. The waves-in-ice amplitude spectrum and the maximal floe size are saved for analysis.

3. Results

[32] Figure 5 shows detailed results for one model run. Figures 5a–5d show the time evolution of the wave amplitude for different periods. Waves propagate unattenuated in ice-free water and are selectively attenuated in the ice, according to the scattering attenuation coefficient. Numerical dispersion tends to broaden the wavefront in time in a period-dependent manner. Since boundary conditions are kept constant throughout the integration ($A^n_{w,j=1} = A_w = constant$), this has no effect on the final result and the slowest wave crosses the entire domain (~500 km) in approximately 12 h. As waves break up the ice, the maximum floe size $D_{\max}$ progressively increases from the ice edge inward (Figure 5e). Short waves that produce small floes are rapidly and exponentially dampened below their yield amplitude. Larger waves attenuate almost linearly due to a progressive decrease in the number of floes per unit distance. Eventually, all waves are attenuated below their yield amplitude, which increases with ice thickness (Figure 5f), and fragmentation stops. Beyond this point, the attenuation rate stabilizes and settle to a thickness-dependent value with $\overline{D}$ = 500 m.

[33] We define the MIZ as ice with floe sizes below 200 m, which corresponds to half the wavelength of the longest wave (T = 15.9 s). Figure 5e shows how the MIZ and its extent L_{MIZ} are defined. One interesting result can readily be noted: the model produces a sharp transition between the MIZ and the inner ice pack. This result mirrors what is usually observed in Fram Strait (Figure 1) and provides an interesting criterion for distinguishing ice dynamical regimes. As we chose a small value for ΔT = 0.3 s, this result is likely to be independent of the spectral resolution and represents well the physical response of the system. In section 3.1, we look at how the extent of the MIZ varies when environmental conditions and ice mechanical properties change.

3.1. Model Sensitivity in Idealized Conditions

[34] As seen in sections 2.2 and 2.3, ice thickness and wave period are expected to be the two most determinant factors of

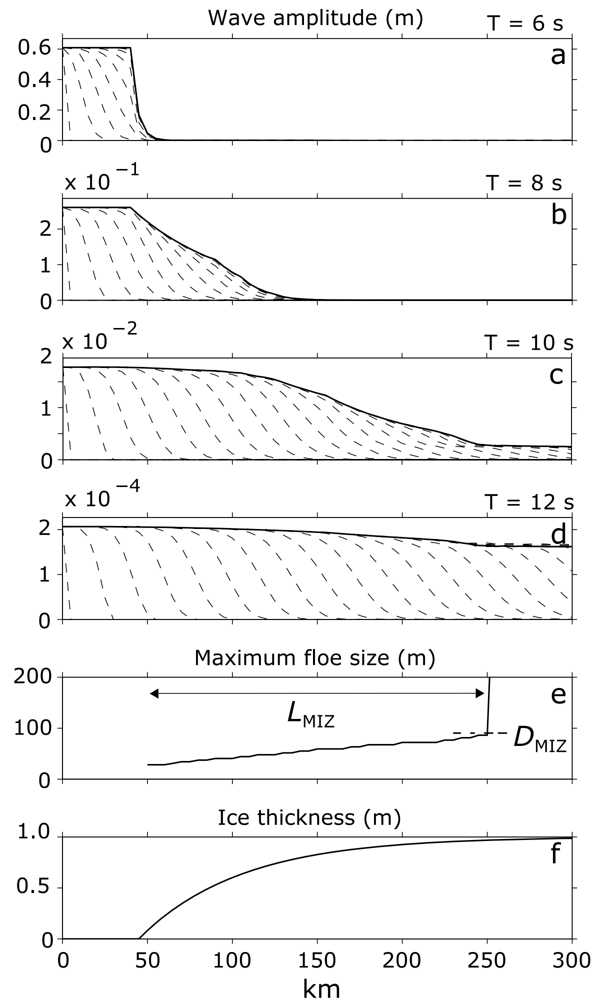

Figure 5. Wave advection and attenuation of wave amplitude for different periods: (a) 6, (b) 8, (c) 10, and (d) 12 s. Initial values correspond to a Pierson-Moskowitz spectrum with T_p = 6 s. Dashed lines show wave amplitude at every five time steps (Δt = 400 s). The solid line represents the final stationary wave amplitude. (e) Maximum floe size and (f) ice thickness are also shown. The marginal ice zone is defined as the portion of the cover where the floe size does not exceed 200 m.

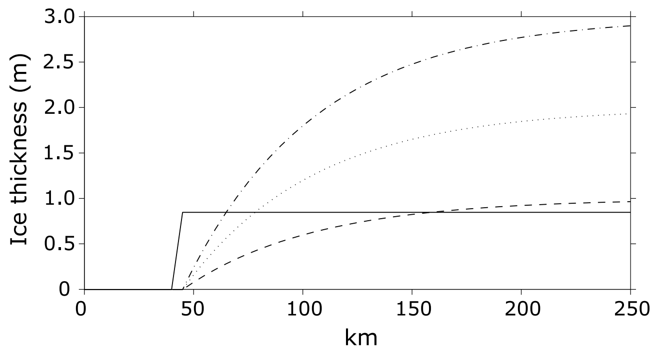

Figure 6. Thickness profiles used in the idealized experiments: one constant thickness profile h_0 = 0.85 m (dashed line) and three exponential profiles of the form $h = h_{\mathrm{sat}}$ (1 − exp(x[km]/60)) with h_{sat} = 1.0, 2.0, and 3.0 m (solid line).

the MIZ extent through how they affect floe breaking and wave attenuation. To quantify model sensitivity to ice thickness, we prescribe different profiles, three exponential profiles with different saturation values (1, 2, and 3 m) and one profile with constant thickness (0.85 m, Figure 6). We prescribe a Pierson-Moskowitz wave amplitude spectrum with peak periods ranging from 4 to 10 s. Finally, two different values of ice strength are used to capture the variability of sea ice brine content [*Timco and O'Brien*, 1994]. Strong and weak ice are defined by specifying different flexural strength values: σ_c = 0.95 MPa for strong ice and σ_c = 0.67 MPa for weak ice.

[35] Figure 7 shows how the extent of the MIZ and the maximum floe size vary as a function of these three parameters. The ice strength has a small influence on the extent of the MIZ (typically between 5 to 25%). The peak period of the wave spectrum and the ice thickness are the most important factors affecting the ice breaking penetration distance. It increases exponentially with the peak period and it is highly influenced by the thickness of the ice cover. For a constant thickness profile, short waves are strongly damped near the ice edge so that L_{MIZ} stays small for short peak periods, but diverges quickly when longer waves kick in. When T_p reaches 8–9 s and sea ice thickness is less than 2.0 m, floe breaking occurs over a thousand kilometers. Such conditions are typically found in the Southern Ocean where fully developed seas impact on a first-year ice cover with typical thicknesses between 0 and 2 m [*Worby et al.*, 2008]. Experiments with two different fragility values (f = 0.6 and 0.9) were also performed, and produced variations comparable to those associated with changes in ice strength (not shown), confirming again that ice thickness and wave energy are the main factors determining the extent of the MIZ. More specifically, swells longer than 8–10 s have the most significant impact.

[36] The maximum floe size at the inner boundary increases linearly with the peak period independently of ice thickness and flexural strength (Figures 7c and 7d). In all simulations the MIZ is defined by a step-like progression of the maximum

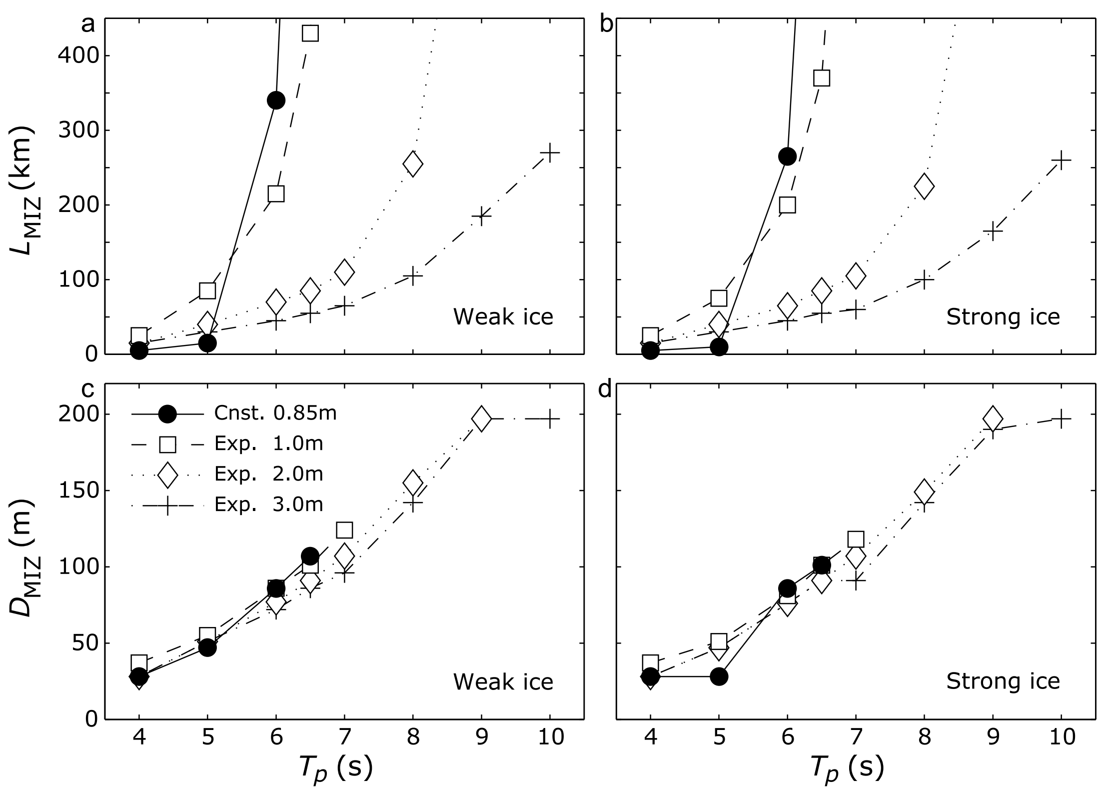

Figure 7. (a, b) Extent of the MIZ, L_{MIZ}, as a function of the Pierson-Moskowitz peak period for different ice thickness profiles (see Figure 6). (c, d) Floe size at the inner boundary D_{MIZ}, which also corresponds to the maximum value across the MIZ. Schematic representations of L_{MIZ} and D_{MIZ} are shown in Figure 5. Results for weak ice (σ_c = 0.67 MPa, Figures 7a and 7c). Results for strong ice (σ_c = 0.95 MPa, Figures 7b and 7d).

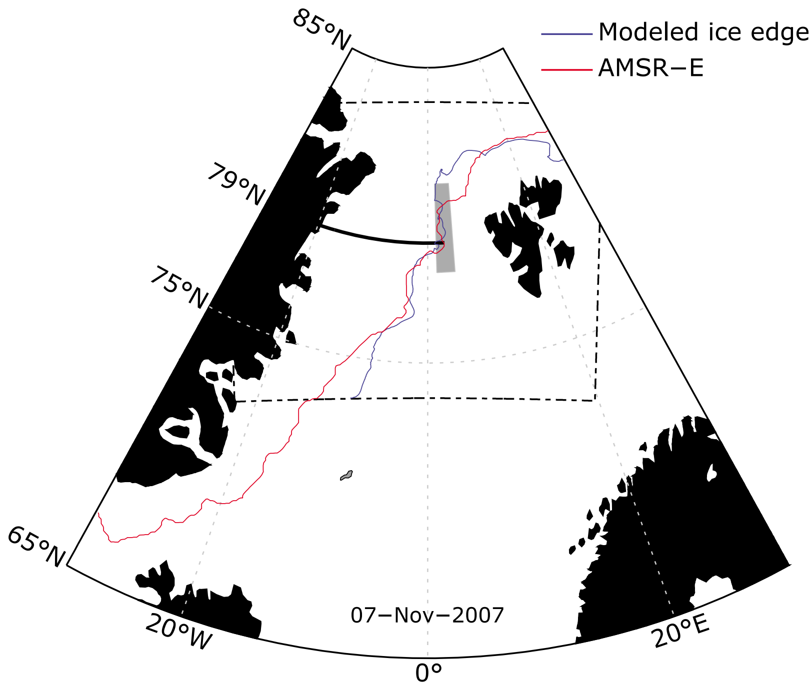

Figure 8. Map of the Fram Strait area showing the observed (red line) and simulated (blue line) ice edges on 7 November 2007. The thick black line along 79°N shows the location where the ice parameters were extracted for the simulations. The gray box shows the grid cell where ocean wavefields were extracted from the ERA-Interim reanalysis. The domain of the Hybrid Coordinate Ocean Model (HYCOM) model of Fram Strait is identified by the dashed line.

floe size (see Figure 5 for one example) even though nothing is prescribed in the formulation of the model that could produce such behavior. Beyond the inner boundary of the MIZ, long waves continue to propagate without breaking the ice, attenuate less due to a smaller number of floes, and could retain enough energy to break thin ice encountered on their path.

3.2. Application to Fram Strait

[37] The model is applied here using more realistic ice thickness profiles. These profiles come from the output of a high-resolution (3.5 km) sea ice-ocean model covering the Fram Strait and the Greenland Sea. The model is a nested configuration of the Hybrid Coordinate Ocean Model (HYCOM) receiving boundary conditions from the TOPAZ system [*Bertino and Lisæter*, 2008]. This model gives a good representation of the ice edge position between 76°N and 81°N (Figure 8). A transect along the 79°N parallel is chosen to carry the simulation. The MIZ in this area is maintained by waves developed in the North Atlantic and the Nordic Seas regularly impacting the ice edge. The Fram Strait is of particular interest as it is the deepest connection between the Arctic and the Atlantic and the waterway through which most ice is exported from the Arctic. Generally, three ice types can be distinguished in Fram Strait: a MIZ near the edge where thickness increases progressively; a central region where ice is thickest and mainly composed of multiyear ice drifting southward from the Arctic; a band of landfast ice along the coast of Greenland where thickness is mostly limited by thermodynamic growth.

[38] The modeled thickness represents these three regions well, although ice along the coast is not landfast. However, with maximum thicknesses of ~2 m across the transect, we suspect that the model underestimates the thickness of multiyear ice in the central part. Time series of upward looking sonar data placed on the shelf break along 79°N in Fram Strait over a 10 year period show monthly averaged values oscillating between 1 and 5 m, with a mean value around 3 m [*Widell et al.*, 2003]. The model thus underestimates ice thickness. To account for such bias, we carry two simulations, one with the original model output and one where thickness is doubled (noted in the colorbar of Figure 9), acknowledging that the general spatial variability is well represented. Ice concentration is the same for both simulations.

[39] For the incident wave energy, we use Bretschneider's two-parameter wave spectrum. The 6 hourly averaged parametric data (H_s and T_p) are extracted from the Wave Model (WAM) operated by the Environmental Center for Medium-Range Weather Forecasting (ECMWF). In order to have a conservative estimate of the MIZ extent, i.e., the maximum penetration of waves, we take the maximum daily value and assume that waves are traveling inward along the transect. Then we proceed with the same approach described in section 3. Ice and wave conditions are updated every day and the floe size is reinitialized so that the system has no memory of the previous day's MIZ. Although unrealistic, the resulting time series of the floe breaking penetration distance during a complete seasonal cycle allow us to assess how variable this process is with changing ice and wave conditions.

[40] Figure 9 shows the results for both simulations. The MIZ is represented by the colored area in Figures 9d and 9e, while the black color represents unbroken ice. The MIZ extent varies strongly with respect to wave energy, but values remain in a realistic range. Although some wave events are

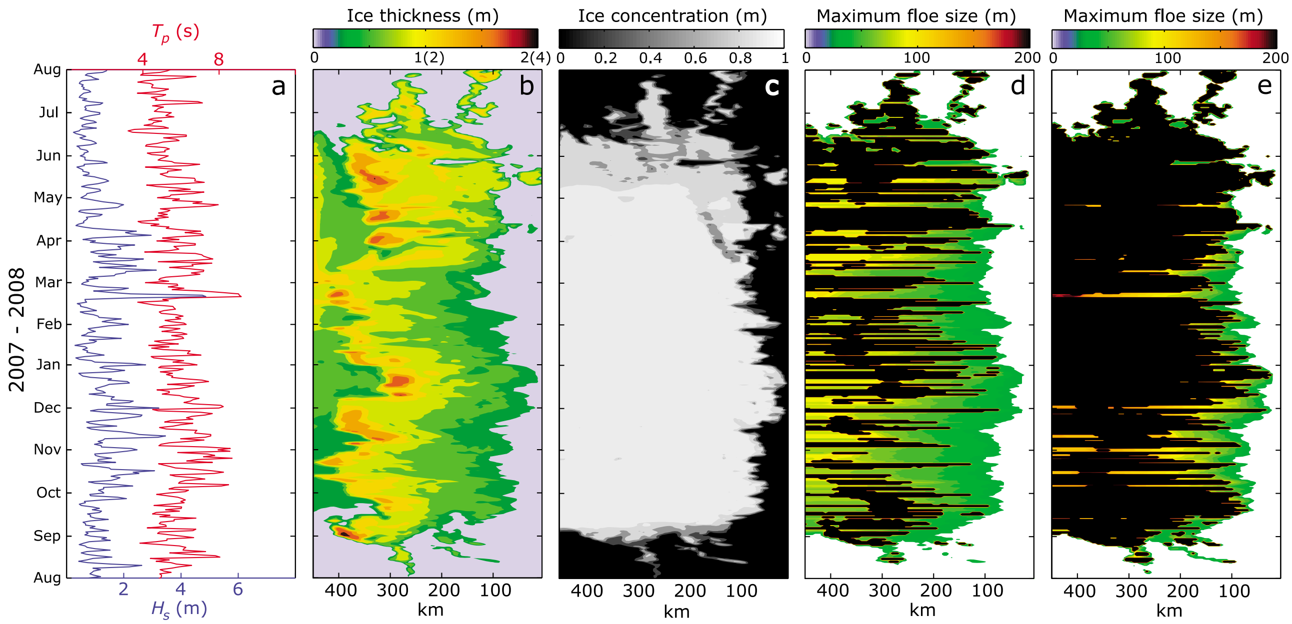

Figure 9. (a) Maximum daily wave spectrum parameters from the Environmental Center for Medium-Range Weather Forecasting (ECMWF) ERA-Interim reanalysis, (b) ice thickness, and (c) ice concentration extracted from the HYCOM Fram Strait model. The ice thickness colorbar has two sets of labels corresponding to the two experiments: (0–2 m) for the original model thicknesses and (0–4 m) for doubled thicknesses. Maximum floe size predicted by the waves-in-ice model (d) with original ice thickness output and (e) with doubled ice thickness. Waves propagate from right to left.

able to break the ice all the way up to the coast of Greenland, the average MIZ extent is 110 km for the original and 59 km for doubled thickness experiment. Complete breakup happens less frequently in the second simulation (Figure 9e). As suggested before, ice breaking effectively happens in isolated areas within the ice pack when waves carry enough energy and hit thin ice areas.

3.3. An Empirical Method for Segregating Ice Dynamical Regimes

[41] One goal of this model is to segregate two ice dynamical regimes based on floe size. However, this strategy could be costly and difficult to implement in coupled climate models. In this section we explore a way to empirically determine where the frontier between the two regimes is located in a sea ice model's parameter space (equivalent ice thickness and concentration). Results obtained in section 3.2 can be viewed as many independent realizations of waves-in-ice experiments done in realistic conditions representing the Fram Strait area. We know already that thin ice is more easily broken up by waves, first because it is less resistant to flexural failure, but also because thin ice is mostly present in the margins of the ice cover. It is then natural to ask whether there are critical thickness and concentration values above which sea ice is rarely broken up by waves and below which sea ice is likely to be broken up. Such a criterion, if it exists, could be used to select in which dynamical regime sea ice is (viscous-plastic or collisional) to better simulate MIZ dynamics.

[42] For this, we use the simulation where sea ice thickness has been doubled simply because it covers a larger portion of thickness-concentration parameter space. Then, we consider ice as fragmented when $D_{max} < D_{limit}$. If D_{limit} is chosen to be small enough (D_{limit} = 30 m), the criterion is likely to be independent of strong wave events during which any type of ice can be fragmented. Figure 10 shows a scatterplot of all ice points in the thickness-concentration parameter space. The red points are considered to be fragmented and in a weak MIZ regime. Blue points represent an energetic MIZ regime where D_{limit} = 200 m. One can see that ice within the MIZ is

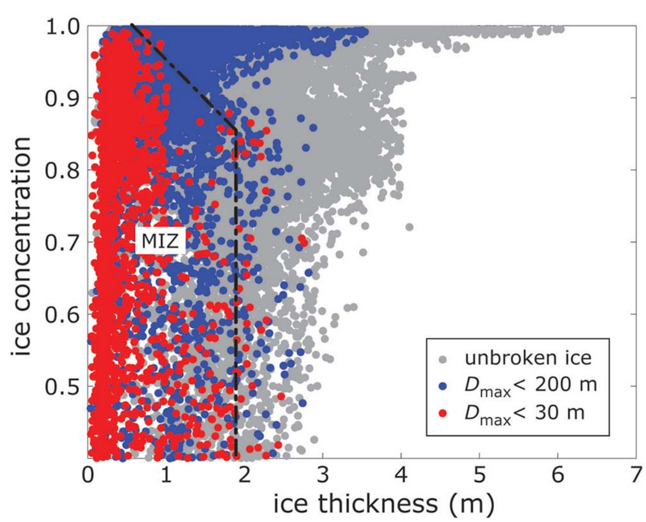

Figure 10. Sea ice fragmentation state of the second simulation represented in the thickness-concentration parameter space. Red dots represent D_{max} < 30 m, blue dots represent D_{max} < 200 m, and gray dots represent unbroken ice. The dashed line sketches a possible boundary between MIZ and viscous-plastic (VP) dynamical regimes.

rarely thicker than ~2 m. This maximum thickness sharply decreases to around 1 m when $c > 0.89$. The dashed line of Figure 10 delineates a portion of the parameter space where fragmentation is likely to occur. In fact, it occurs 59 to 74% of the time, depending on D_{limit}. This empirical analysis is only valid in Fram Strait and does not constitute a universal criterion. It provides an economic way to include and test MIZ-related parameterizations without implementing waves in ice explicitly. Nonetheless, we believe that the present work makes a significant step toward the explicit inclusion of waves-in-ice processes in sea ice models.

4. Conclusion

[43] A model incorporating a parameterization for the ice breaking due to the presence of waves in ice and the input from a scattering model is used to evaluate the extent of the MIZ and the maximum floe size. In general, the model reproduces standard conceptions of wave-ice interactions in a marginal ice zone: (1) the floe size distribution is under the direct control of waves, (2) floe size increases inward as waves attenuate, and (3) waves are selectively attenuated. Two new results appear from the simple physical considerations at the basis of the model presented here. First, the model predicts a sharp transition between the MIZ and the inner ice pack. It suggests that, in some specific areas like Fram Strait, where this sharp transition is often observed, model validation would become possible by combining wave data (from model or observations), ice type signature from synthetic aperture radar (SAR) orbiting sensors, and freeboard data from CryoSat, indicative of thickness. Second, the discontinuous floe breaking response (Figure 2) supports the idea that two different mechanisms act differently in different conditions. Observations of floe size distributions in the MIZ also suggest a change of regime, which appears as a discontinuity in the distribution [*Toyota et al.*, 2011]. The existence of a link between these two discontinuities is only speculative at this stage, but second-order effects such as wave modulation, and time-dependent floe breaking could be considered to find if the apparent connection bears physical sense.

[44] By applying this model in various environmental conditions, we were able to estimate the extent of the MIZ and explore the model sensitivity. Ice thickness and incident wave energy are the most important factors affecting the extent of the MIZ while sea ice mechanical properties play a secondary role. This is also supported by the nonlinear dependence of the model to ice thickness and wave period, while ice properties affect linearly floe breaking and do not affect wave attenuation. This sensitivity suggests that a decrease of ice thickness or an increase of storm intensity, as it is expected in the Arctic, may significantly increase the extent of the MIZ. In the event that waves impacting the ice edge are sufficiently energetic and the ice cover is relatively thin (<2 m), ice can be broken over hundreds of kilometers. This is typically the case in the Antarctic. The Arctic Ocean is naturally protected from waves by landmasses and islands and wave growth is limited by short fetch. However, with the gradual loss of summer ice in the Canada Basin and over the Siberian Shelf, the summer ice cover will be increasingly pummeled by waves developing in ice-free waters. Consequences of the ice retreat on air-ocean heat and momentum exchanges and on the stability of the upper oceanic layer are still unknown, but waves are definitely expected to play an important role.

[45] When applied in a realistic representation of the Fram Strait, the model provides reasonable predictions for the extent of the MIZ. In the absence of quantitative data against which results can be compared, we argue that it is in fact reasonable based on two things: it predicts the presence of a clearly delimited MIZ, and it predicts that waves do not systematically break up the ice all the way to the coast of Greenland. In the latter case, observations tell us that a wide sheet of level ice is stably attached to land throughout the winter at 79°N. In the first simulation, the one that uses the original ice thickness output, the MIZ does reach the coast quite frequently, while the second simulation, when the thickness is doubled, better fits the observations and complete fragmentation is less frequent. Moreover, a number of factors need to be considered when these results are interpreted: the incident wave energy propagates along the transect while in reality, waves propagate in different directions and thus travel longer distances to reach a given point in the ice pack; a parametric representation for the incident wave spectrum was used, which tends to overestimate the amplitude of large waves; and scattering is considered to be the dominant attenuation mechanism and other sources of wave energy loss are neglected. In summary, the MIZ extent simulated here represents a conservative estimation and further validation is necessary to refine the model.

[46] The model was designed in order to facilitate its implementation in a sea ice model. In addition to floe size, the model also provides the waves-in-ice spectrum as a prognostic output. These variables are of great interest for persons operating and working on sea ice. Coupled with operational wave forecasts, a two-dimensional waves-in-ice model would provide crucial information for the design of infrastructures in ice-covered seas and for the real-time safety of operations. It can also be applied in areas where landfast ice is present and subject to break up by waves in ice coming for great distances. In a two-dimensional world, the directional spectrum of waves and the advection of floe size will be included for a more realistic representation of the MIZ. This will allow a more direct comparison with satellite observations and a direct coupling with dynamical and thermodynamical aspects of sea ice.

[47] This one-dimensional implementation helped to identify a number of limitations that could be prioritized in the future. They include the following:

[48] 1. Wave attenuation is solely determined by scattering. Other types of losses can also play a role, especially for unbroken ice where scattering may occur at ridges and leads instead of floe edges. The attenuation coefficient, here based on KM's model, could be improved by adding other sources of losses (floe collisions, hysteresis, turbulence, pancake or grease ice, etc.) and by considering three-dimensional scattering [e.g., *Bennetts et al.*, 2010].

[49] 2. The expression for the wave amplitude does not consider the effect of modulation when many waves of different but similar periods are present.

[50] 3. The floe breaking parameterization lies on an intuitive conception of flexural failure, which can prove to be more complex in reality. Even though the phenomenon is difficult to observe and measure in situ, the model can be used to test other parameterizations and compare the results

with qualitative if not quantitative in situ or laboratory data. A floe breaking parameterization based on the thin elastic plate theory would provide a more coherent formulation of the problem. At least, a framework within which such a theory would need to fit to specifically simulate floe size- and wave-dependent processes in sea ice models has been proposed here.

[51] **Acknowledgments.** This work was realized within the term of the contract 4100P07.056 funded by Total E&P and as part of the Waves-in-Ice Forecasting for Arctic Operators (WIFAR) project, collaboratively funded by Total E&P and the Research Council of Norway through the Program for Optimal Management of Petroleum Resources (PETROMAKS). A. Kohout is funded by New Zealand's Foundation for Science, Research and Technology (FSRT). The authors wish to thank L. G. Bennetts, V. Squire, Ø. Breivik, I. Keghouche, M. Meylan, and one anonymous reviewer for useful discussions and comments that helped improve the manuscript.

References

Allegre, C. J., J. L. Le Mouel, and A. Provost (1982), Scaling rules in rock fracture and possible implications for earthquakes prediction, *Nature*, *297*, 47–49.

Bennetts, L. G., M. A. Peters, V. A. Squire, and M. H. Meylan (2010), A three-dimensional model of wave attenuation in the marginal ice zone, *J. Geophys. Res.*, *115*, C12043, doi:10.1029/2009JC005982.

Bertino, L., and K. A. Lisæter (2008), The TOPAZ monitoring and prediction system for the Atlantic and Arctic oceans, *J. Oper. Oceanogr.*, *1*, 15–19.

Feltham, D. L. (2005), Granular flow in the marginal ice zone, *Philos. Trans. R. Soc. A*, *363*, 1677–1700.

Goodman, D. J., P. Wadhams, and V. A. Squire (1980), The flexural response of a tabular ice island to ocean swell, *Ann. Glaciol.*, *1*, 23–27.

Hakkinen, S. (1986), Coupled ice-ocean dynamics in the marginal ice zone, *J. Geophys. Res.*, *91*, 819–832.

Haskell, T. G., W. H. Robinson, and P. J. Langhorne (1996), Preliminary results from fatigue tests on in situ sea ice beams, *Cold Reg. Sci. Tech.*, *24*, 167–176.

Hibler, W. D. (1979), A dynamic thermodynamic sea ice model, *J. Phys. Oceanogr.*, *9*, 815–846.

Janssen, P. (2004), *The Interactions of Ocean Waves and Wind*, Cambridge Univ. Press, Cambridge, U. K.

Jenkins, A. D. (2007), The interaction of ocean surface processes, waves, and turbulence in the adjacent boundary layers, in *Transport at the Air-Sea Interface: Measurements, Models and Parametrizations*, edited by C. S. Garbe, R. A. Handler, and B. Jähne, pp. 145–158, Springer, Berlin.

Kohout, A. L. (2008), Water wave scattering by floating elastic plates with application to sea-ice, Ph.D. thesis, Univ. of Auckland, Auckland, New Zealand.

Kohout, A. L., and M. H. Meylan (2008), An elastic plate model for wave attenuation and ice floe breaking in the marginal ice zone, *J. Geophys. Res.*, *113*, C09016, doi:10.1029/2007JC004434.

Lange, M. A., S. F. Ackley, and P. Wadhams (1989), Development of sea ice in the Weddell Sea, *Ann. Glaciol.*, *12*, 92–96.

Langhorne, P. J., V. A. Squire, C. Fox, and T. G. Haskell (1998), Break-up of sea ice by ocean waves, *Cold Reg. Sci. Tech.*, *27*, 438–442.

Liu, A. K., and E. Mollo-Christensen (1988), Wave propagation in a solid ice pack, *J. Phys. Oceanogr.*, *18*, 1702–1712.

Marko, J. R. (2003), Observations and analyses of an intense waves-in-ice event in the Sea of Okhotsk, *J. Geophys. Res.*, *108*(C9), 3296, doi:10.1029/2001JC001214.

Masson, D., and P. Leblond (1989), Spectral evolution of wind-generated surface gravity waves in a dispersed ice field, *J. Fluid Mech.*, *202*, 43–81.

Meylan, M. (2002), The wave response of ice floes of arbitrary geometry, *J. Geophys. Res.*, *107*(C1), 3005, doi:10.1029/2000JC000713.

Meylan, M., and V. A. Squire (1994), The response of ice floes to ocean waves, *J. Geophys. Res.*, *99*, 891–900.

Meylan, M., and V. A. Squire (1996), Response of a circular ice floe to ocean waves, *J. Geophys. Res.*, *101*, 8869–8884.

Meylan, M., V. A. Squire, and C. Fox (1997), Towards realism in modeling ocean wave behavior in marginal ice zones, *J. Geophys. Res.*, *102*, 22,981–22,991.

Ochi, M. K. (1998), *Ocean Waves: The Stochastic Approach*, 332 pp., Cambridge Univ. Press, Cambridge, U. K.

Palmer, A. C., and T. J. O. Sanderson (1991), Fractal crushing of ice and brittle solids, *Proc. R. Soc. A*, *433*, 469–477.

Pierson, W. J., and L. Moskowitz (1964), A proposed spectral form for fully-developed wind seas based on the similarity theory of S. A. Kitaigorodskii, *J. Geophys. Res.*, *69*, 5181–5190.

Røed, L. P., and J. J. O'Brien (1981), Geostrophic adjustment in highly dispersive media: An application to the marginal ice zone, *J. Geophys. Astrophys. Fluid Dyn.*, *18*, 263–278.

Røed, L. P., and J. J. O'Brien (1983), A coupled ice-ocean model of upwelling in the marginal ice zone, *J. Geophys. Res.*, *88*, 2863–2872.

Rothrock, D. A., and A. S. Thorndike (1984), Measuring the sea ice floe size distribution, *J. Geophys. Res.*, *89*, 6477–6484.

Schwarz, J., R. M. W. Frederking, V. Gavrillo, I. G. Petrov, K.-I. Hirayama, M. Mellor, P. Tryde, and K. D. Vaudrey (1981), Standardized testing methods for measuring mechanical properties of ice, *Cold. Reg. Sci. Tech.*, *4*, 245–253.

Shen, H. H., W. D. Hibler, and M. Leppäranta (1986), On applying granular flow theory to a deforming broken ice field, *Acta Mech.*, *63*, 143–160.

Shen, H. H., W. D. Hibler, and M. Leppäranta (1987), The role of floe collisions in sea ice rheology, *J. Geophys. Res.*, *92*, 7085–7096.

Shen, H. H., S. F. Ackley, and M. A. Hopkins (2001), A conceptual model for pancake-ice formation in a wave field, *Ann. Glaciol.*, *33*, 361–367.

Shen, H. H., S. F. Ackley, and Y. Yuan (2004), Limiting diameter of pancake ice, *J. Geophys. Res.*, *109*, C12035, doi:10.1029/2003JC002123.

Squire, V. A. (1981), Numerical simulation of ice floes in waves, *Tech. Rep. 81-1*, 57 pp., Scott Polar Res. Inst., Cambridge, U. K.

Squire, V. A. (2007), Of ocean waves and sea-ice revisited, *Cold. Reg. Sci. Tech.*, *49*, 110–133.

Squire, V. A., J. P. Dugan, P. Wadhams, P. J. Rottier, and A. K. Liu (1995), Of ocean waves and sea-ice, *Ann. Rev. Fluid Mech.*, *27*, 115–168.

Steele, M. (1992), Sea ice melting and floe geometry in a simple ice-ocean model, *J. Geophys. Res.*, *97*, 17,729–17,738.

Steele, M., J. H. Morrison, and N. Untersteiner (1989), The partition of air-ocean momentum exchange as a function of ice concentration, floe size, and draft, *J. Geophys. Res.*, *94*, 12,739–12,750.

Steer, A., A. P. Worby, and P. Heil (2008), Observed changes in sea-ice floe size distribution during early summer in the western Weddell Sea, *Deep Sea Res. Part II*, *55*, 933–942.

Timco, G. W., and S. O'Brien (1994), Flexural strength equation for sea ice, *Cold Reg. Sci. Tech.*, *22*, 285–298.

Timoshenko, S., D. H. Young, and W. Weaver Jr. (1974), *Vibration Problems in Engineering*, 4th ed., John Wiley, New York.

Toyota, T., S. Takatsuji, and T. Nakayama (2006), Characteristics of sea ice floe size distribution in the seasonal ice zone, *Geophys. Res. Lett.*, *33*, L02616, doi:10.1029/2005GL024556.

Toyota, T., C. Haas, and T. Tamura (2011), Size distribution and shape properties of relatively small sea-ice floes in the Antarctic marginal ice zone in late winter, *Deep Sea Res. II*, doi:10.1016/j.dsr2.2010.10.034, in press.

Turcotte, D. L. (1986), Fractals and fragmentation, *J. Geophys. Res.*, *91*, 1921–1926.

Wadhams, P. (1986), The seasonal ice zone, in *The Geophysics of Sea Ice*, edited by N. Untersteiner, pp. 825–991, Plenum, New York.

Wadhams, P., V. A. Squire, D. J. Goodman, A. M. Cowan, and S. C. Moore (1988), The attenuation rates of ocean waves in the marginal ice zone, *J. Geophys. Res.*, *93*, 6799–6818.

Widell, K., S. Østerhus, and T. Gammelsrød (2003), Sea ice velocity in the Fram Strait monitored by moored instruments, *Geophys. Res. Lett.*, *30*(19), 1982, doi:10.1029/2003GL018119.

Worby, A. P., C. A. Geiger, M. J. Paget, M. L. Van Woert, S. F. Ackley, and T. L. DeLiberty (2008), Thickness distribution of Antarctic sea ice, *J. Geophys. Res.*, *113*, C05S92, doi:10.1029/2007JC004254.

World Meteorological Organization (WMO) (1998), *Guide to Wave Analysis and Forecasting*, 2nd ed., Geneva, Switzerland.

L. Bertino, Nansen Environmental and Remote Sensing Center, Thormøhlensgate 47, N-5006, Bergen, Norway.

D. Dumont, Institut des Sciences de la Mer, Université de Québec à Rimouski, 310 Allée des Ursulines, Rimouski, Québec G5L 3A1, Canada. (dany_dumont@uqar.ca)

A. Kohout, National Institute of Water and Atmospheric Research, 10 Kyle St., Christchurch 8011, New Zealand.